

# Electrostatics of a Finite Conducting Cylinder: Elliptic-Kernel Integral Equation and Capacitance Asymptotics

J. Ricardo de Sousa  
Universidade Federal do Amazonas,  
Departamento de Física,  
3000, Japiim, 69077-000, Manaus-AM, Brazil.

## Abstract

We study the electrostatics of a thin, finite-length conducting cylindrical shell held at constant potential  $V_0$ . Exploiting axial symmetry, we recast the problem as a one-dimensional singular integral equation for the axial surface-charge density, with a kernel written in terms of complete elliptic integrals. A Chebyshev-weighted collocation scheme that incorporates the square-root edge singularity yields rapidly convergent charge profiles and dimensionless capacitances for arbitrary aspect ratios  $L/a$ , recovering known long- and short-cylinder limits and providing accurate benchmark values in the intermediate regime. The method offers a compact, numerically robust reference formulation for the electrostatics of finite cylindrical conductors.

## 1 Introduction

The electrostatics of finite conductors remains a canonical benchmark for both analytical methods in potential theory and high-accuracy numerical solvers. Among such geometries, the finite right-circular cylinder, equivalently, an open conducting tube, occupies a particularly important position, as it continuously interpolates between two singular limits: the slender-body regime, characterized by weak axial variation of the surface charge except near the ends, and the short-cylinder or ring-like regime, in which a vanishing length at fixed radius leads to behavior dominated by rim effects.

The capacitance and surface-charge distribution of finite-length cylinders constitute a classic electrostatic problem that admits no closed-form solution in elementary functions and has therefore been investigated extensively by numerical and semi-analytical means. Early experimental and theoretical interest dates back to classical capacitance measurements and bounds associated with Cavendish and Maxwell [1, 2]. Since then, the problem has remained a stringent test case, combining axial symmetry with a nontrivial edge singularity that challenges both analysis and computation [3].

As a result, the open-cylinder geometry has attracted sustained attention in the applied-electromagnetics and electrostatics communities. Mid-twentieth-century studies employed boundary-integral and matrix methods, producing numerical data and practical approximations across wide ranges of aspect ratio. In this context, the work of Vainshtein and related contributions by Kapitsa, Fock, and collaborators [4–6] are widely regarded as milestones in the systematic numerical analysis of hollow finite cylinders [7]. Subsequent developments included dual integral equation formulations, often reducible to linear systems via Neumann-series-type constructions, method-of-moments implementations, and semi-empirical parameterization for engineering use. Verolino, in particular, formulated the surface-charge-density problem for a hollow metallic cylinder within the framework of dual integral equations and provided a detailed assessment of classical approximations [8].

Parallel efforts focused on the capacitance of the open cylinder as a global observable. Classical engineering-level formulas and numerical comparisons were reported early on, and later studies refined these approximations and tabulated high-accuracy values spanning both the tube and ring limits. Scharstein’s Capacitance of a Tube is frequently cited in this context, and modern reviews often list it alongside earlier analytical and numerical results [9]. More recent work has proposed analytic and semi-analytic representations that combine explicit singular terms with rapidly convergent expansions, such as Legendre-series constructions, yielding closed-form or near-closed-form expressions consistent with established benchmarks [10–18].

Despite this substantial literature, two practical gaps remain. First, many studies emphasize capacitance values or low-parameter fits, whereas publication-quality, high-resolution surface-charge distributions for a prescribed constant potential are less commonly reported in a form that is directly reproducible and numerically stable across broad aspect ratios. Second, even when charge-density information is available, the integrable endpoint singularity at the rims can obscure convergence analyses unless the discretization explicitly incorporates the correct edge behavior.

From a mathematical standpoint, the difficulty lies not in solving Laplace’s equation itself, but in handling the mixed (dual) boundary character associated with an open surface possessing sharp rims. The surface charge density on a finite cylindrical shell exhibits a universal square-root divergence at the edges, and numerical schemes that fail to encode this behavior explicitly typically converge slowly and may become ill-conditioned. This feature closely parallels the broader literature on charged wires, needles, and thin conductors, where carefully designed benchmark computations were historically required to resolve competing approximations.

In this work, we address these issues for a zero-thickness conducting cylindrical shell of radius  $a$  and finite length  $L$ , held at a uniform potential  $V_0$ . Our primary goal is to construct a numerically robust real-space formulation that resolves the edge singularities and remains well conditioned over a broad range of aspect ratios. To that end, we first derive an exact one-dimensional axisymmetric integral equation in which the surface potential is expressed through a nonlocal operator with a kernel involving complete elliptic integrals, arising from azimuthal integration of ring-to-ring interactions. We then solve this singular integral equation by means of a Chebyshev-weighted collocation scheme that factors out the rim singularity by construction. This yields rapidly convergent, stable solutions for both the surface-charge density and the dimensionless capacitance  $\tilde{C}(\alpha) = C/(2\pi\epsilon_0 a)$ , with  $\alpha = a/L$ , and allows a systematic

finite-size scaling analysis to control discretization errors and extrapolate to the continuum limit. Only after establishing this real-space solution do we revisit the classical Bessel-based dual-integral-equation (spectral) representation and show that it generates exactly the same elliptic-kernel operator, thereby providing an independent analytical validation and clarifying how distinct mathematical approaches encode the same physical content [8].

The paper is organized as follows. In Section 2 we introduce the physical model and derive the elliptic-kernel integral equation governing the axial surface-charge density. In Section 3 we describe the Chebyshev-weighted numerical method. Section 4 discusses numerical results for the surface-charge density and capacitance across a wide range of aspect ratios, including the extrapolation procedure used to obtain continuum-limit results and asymptotic regimes. Section 5 presents the equivalent spectral formulation based on dual integral equations and establishes explicitly the correspondence between the two approaches. Finally, Section 6 summarizes the main conclusions and outlines possible extensions.

## 2 Physical Model and Integral Equation

We consider a thin (zero-thickness) conducting cylindrical shell aligned with the  $z$ -axis, of radius  $a$  and finite length  $L$ , occupying the interval  $-L/2 < z < L/2$ . The conductor is held at a uniform electrostatic potential  $V_0$ , as sketched in Fig. 1. In the absence of external fields, the configuration is axially symmetric; therefore the induced surface-charge density is independent of the azimuthal angle  $\varphi$  and depends only on the axial coordinate, i. e.,  $\sigma(z)$ , for  $\rho = a$  and  $z \in [-L/2, L/2]$ .

The objective of this work is to determine the surface-charge density  $\sigma(z)$  induced on a finite conducting cylindrical shell held at a constant electrostatic potential. Although this is a classical problem in electrostatics, it still warrants further analysis due to its nontrivial mathematical structure and the subtle role played by edge effects.

We employ two complementary analytical approaches. In the first approach, a more direct formulation is adopted, in which the potential is expressed through real-space integral representations involving *complete elliptic integrals*. In the second, a *spectral formulation* is developed by expanding the electrostatic potential in terms of Bessel functions, which naturally leads to a system of dual integral equations for the unknown charge distribution.

We explicitly demonstrate that these two formulations are mathematically equivalent, providing different but consistent perspectives on the same physical problem. This equivalence not only clarifies the underlying structure of the solution but also highlights the connections between spectral methods, nonlocal integral operators, and classical kernel representations in electrostatics.

In cylindrical coordinates, the electrostatic potential at an arbitrary field point  $(\rho, \varphi, z)$  due to a surface-charge density distributed on the lateral surface  $\rho' = a$  is

$$\Phi(\rho, z) = k_e \int_{-L/2}^{L/2} \int_0^{2\pi} \frac{\sigma(z') adz' d\varphi'}{\sqrt{\rho^2 + a^2 + (z - z')^2 - 2a\rho \cos(\varphi - \varphi')}}, \quad (1)$$

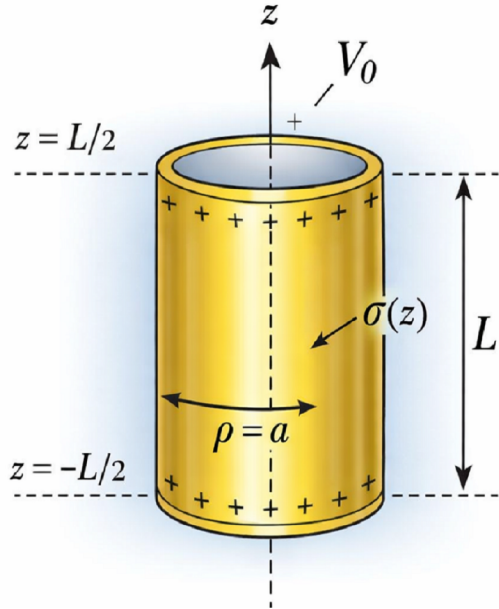


Figure 1: Schematic representation of a thin conducting cylindrical shell of radius  $a$  and finite length  $L$ , aligned with the  $z$ -axis and held at a uniform electrostatic potential  $V_0$ . The cylinder occupies the region  $-L/2 < z < L/2$  and has zero thickness. Owing to axial symmetry and the absence of external fields, the induced surface-charge density is independent of the azimuthal angle and depends only on the axial coordinate,  $\sigma = \sigma(z)$ , on the surface  $\rho = a$ .

where  $k_e = 1/(4\pi\epsilon_0)$  is the electrostatic constant. Since  $\sigma(z')$  is independent of  $\varphi'$ , the azimuthal integral can be performed analytically in terms of the complete elliptic integral of the first kind  $K(m)$ , yielding

$$\Phi(\rho, z) = 4k_e a \int_{-L/2}^{L/2} \sigma(z') \frac{K[m(z')]}{\sqrt{(\rho + a)^2 + (z - z')^2}} dz', \quad (2)$$

with

$$K[m(z')] = \int_0^{\pi/2} \frac{d\theta}{\sqrt{1 - m(z') \sin^2(\theta)}}, \quad (3)$$

and elliptic parameter

$$m(z') = \frac{4a\rho}{(\rho + a)^2 + (z - z')^2}. \quad (4)$$

Imposing the Dirichlet boundary condition on the conductor,  $\Phi(a, z) = V_0$ , Eq. (2) reduces to the integral equation

$$\int_{-L/2}^{L/2} \sigma(z') \mathcal{G}(z - z') dz' = \frac{\pi\epsilon_0}{a} V_0, |z| < L/2, \quad (5)$$

where the kernel is

$$\mathcal{G}(q) = \frac{K\left(\frac{4a^2}{4a^2+q^2}\right)}{\sqrt{4a^2 + q^2}}. \quad (6)$$

Equation (5) is precisely the mathematical core of the problem: determine  $\sigma(z)$  such that the convolution with  $\mathcal{G}(q)$  is constant over  $|z| < L/2$ . The kernel has a weak (logarithmic) singularity as  $q \rightarrow 0$

$$\mathcal{G}(q \rightarrow 0) \simeq \frac{1}{2a} \ln\left(\frac{8a}{|q|}\right) + \mathcal{O}(1), \quad (7)$$

which implies an edge divergence of the surface charge. Near the cylinder ends  $z \rightarrow \pm L/2$ , one expects the generic square-root blow-up [3]

$$\sigma(z) \simeq \frac{\sigma_0}{\sqrt{\left(\frac{L}{2a}\right)^2 - \left(\frac{z}{a}\right)^2}}, \quad (8)$$

where  $\sigma_0$  is a constant with the dimensions of surface-charge density.

### 3 Chebyshev-Weighted Numerical Method

Because of this integrable but strong edge divergence, a naive discretization of Eq. (5) converges slowly and may become numerically ill-conditioned. To stabilize the computation and enforce the correct endpoint behavior by construction, we introduce a Chebyshev-weighted parametrization.

Using the dimensionless coordinate  $x = (2/L)z \in [-1, 1]$ , we rewrite the surface-charge density as

$$\sigma(z) = \frac{1}{\sqrt{1-x^2}} p(x), \quad (9)$$

where the weight  $(1-x^2)^{-1/2}$  captures the expected square-root divergence at  $x = \pm 1$ , while  $p(x)$  remains smooth on  $[-1, 1]$ . When convenient, we represent  $p(x)$  by a truncated *Chebyshev expansion in polynomials* of the first kind  $T_n(x)$  [19–21]

$$p(x) = \sum_{n=0}^N c_n T_n(x), \quad (10)$$

where  $N$  is the **spectral truncation order** and the coefficients  $\{c_n\}$  are obtained numerically. The resulting integral equation is solved by a collocation method combined with Gauss–Chebyshev quadrature, following standard spectral discretization strategies for weakly singular kernels [22–24].

With this transformation, Eq. (5) becomes the following integral equation over  $x$ :

$$\int_{-1}^1 \frac{p(x')}{\sqrt{1-x'^2}} \frac{K\left[\frac{16\alpha^2}{16\alpha^2+(x-x')^2}\right]}{\sqrt{16\alpha^2+(x-x')^2}} = \frac{\pi\epsilon_0}{a} V_0, \quad (11)$$

where  $\alpha = a/L$  is the dimensionless geometric parameter.

We solve Eq. (11) by a Nyström/collocation discretization on  $[-1, 1]$  combined with Gauss–Chebyshev quadrature tailored to the Chebyshev weight. Specifically:

1. **Collocation grid.** We partition the interval  $x \in [-1, 1]$  into  $N_p$  panels and enforce Eq. (11) at a set of collocation points  $\{x_j, j = 1, 2, \dots, N_c\}$  (either the Chebyshev–Lobatto nodes or the panel midpoints mapped to  $[-1, 1]$ ).

2. **Quadrature.** On each panel, the integral over  $x'$  is evaluated using an  $n_g$ –point Gauss–Chebyshev rule, which is naturally adapted to the weight  $(1-x^2)^{-1/2}$ . Here  $n_g$  controls the within-panel quadrature order.

3. **Linear system.** The discretization yields the dense linear system

$$\sum_{j=1}^{N_c} A_{ij} p(x_j) = B_i, \quad (12)$$

where  $N_c$  is the number of collocation conditions (equivalently, the number of unknown nodal values  $p(x_j)$ ). In our implementation we collocate at panel midpoints, so that  $N_c = N_p$ . The matrix entries  $A_{ij}$  are assembled from the elliptic-integral kernel evaluated at these nodes together with the corresponding Gauss–Chebyshev quadrature weights, while  $B_i$  represents the prescribed constant potential. We solve for  $\{p(x_j)\}$  using standard dense linear-algebra routines.

4. **Dimensionless normalization.** We report the dimensionless density  $\tilde{\sigma}(z) = a\sigma(z)/(\epsilon_0 V_0)$ , which removes the trivial dependence on  $V_0$  and  $\epsilon_0$  and isolates the geometric dependence through  $\alpha = a/L$ .

## 4 Numerical Results

In order to illustrate the computations presented below, we discretize the integral equation using  $N_p = 220$  panels in  $x$ , with  $n_g = 16$  Gauss–Chebyshev points per panel. Figure 2 displays  $\tilde{\sigma}(z)$  as a function of the normalized coordinate  $z/L$  for aspect ratios  $\alpha = 1/3, 1.0, 2.0$ , and  $5.0$ . In all cases, the surface-charge density increases monotonically as  $z \rightarrow \pm L/2$ , in agreement with the edge divergence predicted by Eq. (8). As  $\alpha$  increases, that is, as the cylinder becomes shorter, the two ends approach each other in the dimensionless coordinate  $z/L$ , and edge effects penetrate more deeply into the interior region, leading to a higher surface-charge density throughout the cylinder.

At the cylinder center  $z = 0$ , we obtain

$$\begin{cases} \tilde{\sigma}(\alpha = 1/3) \simeq 0.5844 \\ \tilde{\sigma}(\alpha = 1) \simeq 1.1466 \\ \tilde{\sigma}(\alpha = 2) \simeq 1.9160 \\ \tilde{\sigma}(\alpha = 5) \simeq 3.9371 \end{cases} . \quad (13)$$

Beyond the qualitative trends summarized above, the main contribution of the present note is methodological: Eq. (5) provides an exact boundary-integral formulation with an elliptic-integral kernel, but its weak *logarithmic singularity* makes direct discretizations poorly conditioned. By extracting the endpoint behavior analytically through the weighted representation  $\sigma(z) = (1 - x^2)^{-1/2} p(x)$ , the remaining unknown  $p(x)$  becomes smooth and can be determined accurately by collocation with Gauss–Chebyshev quadrature. This produces a stable, rapidly convergent procedure that resolves the edge-dominated regime without ad hoc smoothing or endpoint fitting, and yields a reproducible reference solution for  $\sigma(z)$  at fixed potential.

### 4.1 Finite size-scaling

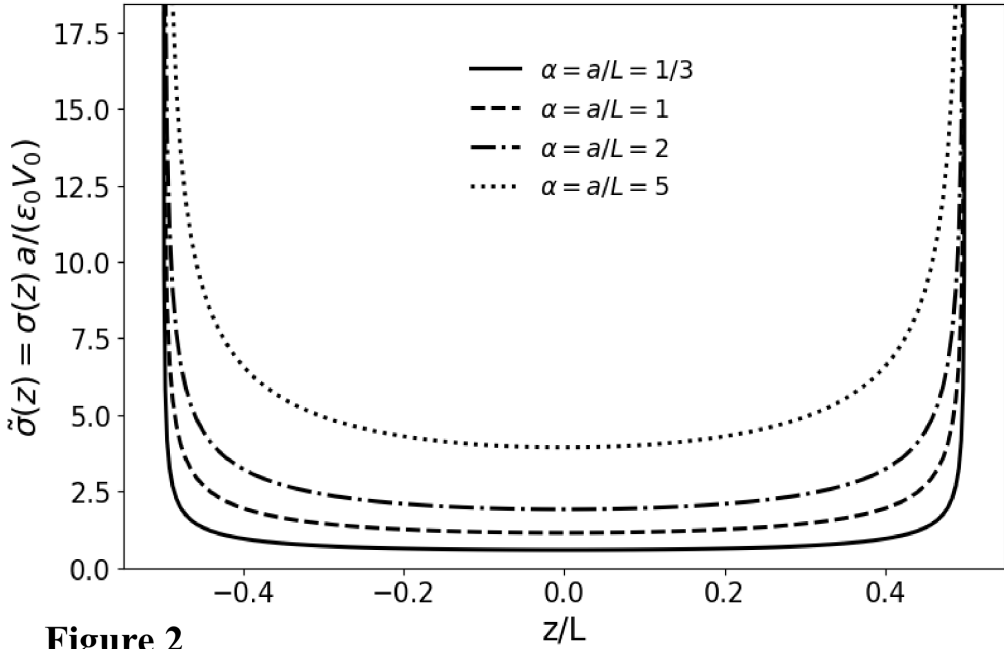
To estimate the continuum-limit value of the center density, we compute  $\tilde{\sigma}(0)$  for a sequence of increasingly refined Chebyshev-panel discretizations, while keeping the quadrature order within each panel fixed. Specifically, for each  $N_c$  we solve the discretized integral equation for the auxiliary unknown  $p(x)$  using  $n_g = 16$  Gauss–Chebyshev points per panel to evaluate the panel integrals. The center value  $\tilde{\sigma}(0)$  is then obtained by interpolation from the collocation nodes.

In the asymptotic regime we fit the data to the leading finite- $N_c$  form

$$\tilde{\sigma}(0, N_c) = \tilde{\sigma}_\infty(0) + \frac{A}{N_c} + \mathcal{O}(N_c^{-2}), \quad (14)$$

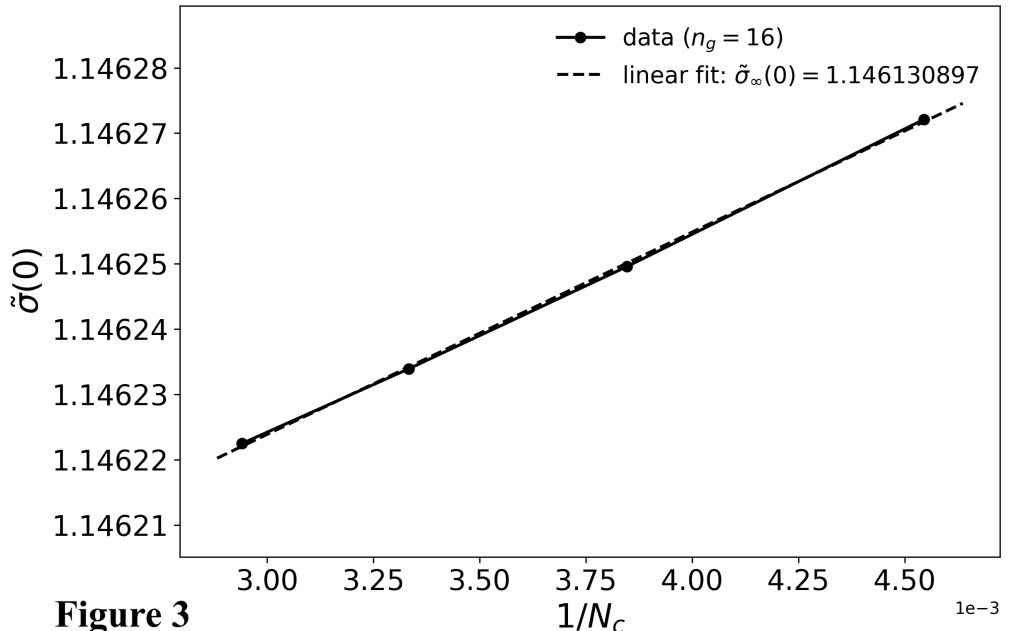
which is equivalent to a linear regression of  $\tilde{\sigma}(0)$  versus  $1/N_c$ . Restricting the fit to sufficiently large  $N_c$  (here  $N_c \geq 220$ ) suppresses pre-asymptotic curvature and yields a stable intercept  $\tilde{\sigma}_\infty(0)$ , which we take as our best estimate of the  $N_c \rightarrow \infty$  limit.

Figure 3 displays a finite-size scaling analysis of the numerical collocation scheme. We plot the cylinder-center density  $\tilde{\sigma}(0)$  as a function of  $1/N_c$ . A least-squares extrapolation based on the sequence of discretizations  $N_c = \{220, 260, 300, 340\}$  yields the converged value  $\tilde{\sigma}_\infty(0) \approx 1.1461309$  for  $\alpha = 1$ . The same extrapolation can be carried out for any aspect ratio  $\alpha = a/L$ . In



**Figure 2**

Figure 2: Dimensionless surface-charge density on the lateral wall of an open conducting cylinder held at a uniform potential  $V_0$ . The curves show  $\tilde{\sigma}(z) = a \sigma(z) / (\epsilon_0 V_0)$  as a function of the normalized axial coordinate  $z/L$ , for four aspect ratios  $\alpha = 1/3, 1, 2$ , and  $5$  (different line styles). The vertical scale is restricted to emphasize the interior region; the rapid rise near  $z/L = \pm 1/2$  reflects the edge (rim) charge crowding at the open ends.



**Figure 3**

Figure 3: Finite-size scaling of the numerically computed cylinder-center surface-charge density. The dimensionless center value  $\tilde{\sigma}(0)$  for  $\alpha = 1$  is plotted versus  $1/N_c$ , where  $N_c$  is the number of Chebyshev panels used in the axial discretization of the integral equation, with within-panel quadrature fixed at  $n_g = 16$  Gauss–Chebyshev points. In the asymptotic regime ( $N_c \geq 220$ ) the data fall on an approximately straight line, consistent with a leading discretization error  $\tilde{\sigma}(0, N_c) = \tilde{\sigma}_\infty(0) + A/N_c + \mathcal{O}(N_c^{-2})$ . The dashed line is the corresponding linear least-squares fit, whose intercept provides the  $N_c \rightarrow \infty$  extrapolation  $\tilde{\sigma}_\infty(0)$ .

practice, we find that the  $N_c \rightarrow \infty$  intercepts differ only weakly from the direct  $N_c = 220$  results: for the range of  $\alpha$  considered in this work, the correction  $\Delta\tilde{\sigma}(0) = |\tilde{\sigma}(0, N_c = 220) - \tilde{\sigma}_\infty(0)|$  is small compared with the overall variation of  $\tilde{\sigma}(0)$  with  $\alpha$ . Thus, while Fig. 3 illustrates the procedure explicitly for  $\alpha = 1$ , the values reported throughout the paper at  $N_c = 220$  already provide an excellent approximation to the extrapolated continuum-limit densities, and the finite- $N_c$  extrapolation mainly serves as a quantitative validation of numerical convergence.

These results are significant because the surface density directly sets the local normal field,  $E_n(z) = \sigma(z)/\varepsilon_0$ , so the computed profiles quantify where the maximum fields occur and how strongly they concentrate near the ends as geometry is varied. In practical electrode design, such end concentrations often determine breakdown and emission thresholds; therefore, an accurate benchmark for  $\sigma(z)$  provides a controlled way to estimate peak-field enhancement in finite cylindrical electrodes. Moreover, the present framework, exact kernel plus endpoint-aware discretization, can be extended with minimal changes to segmented electrodes, nonuniform boundary potentials, or coupled conductor configurations, making it a useful computational template rather than a one-off calculation.

## 4.2 Capacitance

An additional quantity of direct interest that follows directly from the numerical solution for the surface-charge density  $\sigma(z)$  is the self-capacitance of the finite cylindrical conductor. For an isolated conductor held at a uniform potential  $V_0$ , the capacitance provides a compact global measure of the electrostatic response and is particularly useful for comparison with classical results and asymptotic approximations.

We define the geometry-dependent capacitance coefficient  $C_{11} \equiv C(\alpha)$  through the total charge on the lateral surface,

$$C(\alpha) = \frac{1}{V_0} \int_{-L/2}^{L/2} \sigma(z') 2\pi a dz', \quad (15)$$

so that, by construction, the total charge satisfies  $Q = C(\alpha)V_0$ . The corresponding electrostatic self-energy is then given by

$$U(\alpha) = \frac{1}{2} C(\alpha) V_0^2, \quad (16)$$

which provides an energetically meaningful characterization of the system and offers an alternative global diagnostic of the numerical solution.

Because the capacitance integrates the full surface-charge distribution, it is sensitive to both the bulk behavior and the rim singularities, and thus serves as a stringent test of numerical accuracy. Moreover, its dependence on the aspect ratio  $\alpha = a/L$  allows for direct assessment of the crossover between the long-cylinder and short-cylinder regimes, facilitating comparison with known asymptotic results and previously reported benchmark values.

### 4.2.1 Asymptotic Regimes

Before proceeding to the full numerical solution of Eq. (15), it is instructive to examine the physically relevant asymptotic limits of the hollow cylindrical capacitor. These limiting regimes provide valuable insight into the structure of the surface-charge distribution, clarify the origin and role of edge singularities, and serve as analytical benchmarks against which the numerical results can be assessed. In particular, the asymptotic analysis elucidates how the problem interpolates between the long-cylinder (slender-body) limit and the short-cylinder (ring-like) limit, thereby highlighting the distinct physical mechanisms that dominate the electrostatics in each case.

**Long cylinder ( $\alpha \ll 1$ )** In the slender-cylinder limit,  $\alpha \ll 1$  ( $L \gg a$ ), the capacitance shows the familiar logarithmic dependence associated with three-dimensional conductors with a small transverse length scale. A convenient derivation follows from a slender-body approximation: away from the rims the charge varies slowly, so the cylinder may be modeled by a nearly uniform line charge of linear density  $\lambda \simeq Q/L$ . The resulting potential on the surface, evaluated at a representative point (e.g. near the midplane), has the asymptotic form

$$V_0 \simeq \frac{\lambda}{2\pi\epsilon_0} \left[ \ln\left(\frac{2L}{a}\right) - 1 \right], \quad (17)$$

where the dominant  $\ln(2L/a)$  term is universal and the additive constant accounts for end corrections in the three-dimensional geometry (*Maxwell's classical form*) [2]. Solving for  $C = Q/V_0$  yields

$$\tilde{C}(\alpha) = \frac{C(\alpha)}{2\pi\epsilon_0 a} \simeq \frac{(1/\alpha)}{\ln(2/\alpha) - 1}, \quad \alpha \ll 1. \quad (18)$$

This expression highlights the “almost linear” growth of capacitance with the length  $L$  (since  $1/\alpha = L/a$ ), corrected by the slowly varying logarithmic factor  $\ln(2/\alpha)$ . Although  $\ln(2/\alpha) \rightarrow \infty$  as  $\alpha \rightarrow 0$ , it does so only slowly, whereas  $1/\alpha$  grows unbounded; the net effect is a divergence of  $\tilde{C}(\alpha)$  as  $\alpha \rightarrow 0$ , weaker than purely linear scaling but still without bound in the idealized limit.

Below we report representative numerical values of the dimensionless capacitance for  $N_c = 220$ . The results clearly reveal the singular behavior of the capacitance as  $\alpha \rightarrow 0$ , corresponding to the thin, long-cylinder limit. Specifically, we find

$$\left\{ \begin{array}{l} \tilde{C}_\infty(\alpha = 0.1) \simeq 4.96 \\ \tilde{C}_\infty(\alpha = 0.05) \simeq 7.58 \\ \tilde{C}_\infty(\alpha = 0.02) \simeq 14.20 \\ \tilde{C}_\infty(\alpha = 0.01) \simeq 23.73 \end{array} \right. . \quad (19)$$

These values demonstrate the rapid growth of the capacitance as the aspect ratio decreases, reflecting the increasing dominance of end effects and the associated divergence of the surface-charge density in this regime.

Many classic tabulations report the electrostatic capacity of finite cylinders in Gaussian units, where capacitance has dimensions of length and is commonly quoted as  $C/a$  versus  $x = L/a$ . In

particular, Table 1 of Ref. [13] provides high-accuracy benchmark values for the hollow (open) cylinder in the column  $C^{(H)}/a$ . To compare these data with our SI-based normalization, we define the dimensionless capacitance  $\tilde{C}(\alpha) = C_{SI}/(2\pi\epsilon_0 a)$ , with  $\alpha = a/L = 1/x$ , and use the conversion  $C_{SI} = 4\pi\epsilon_0 C_G$ . Since Ref. [13] reports  $C_G/a = C^{(H)}/a$ , the mapping becomes simply  $\tilde{C}(\alpha) = 2C_G/a$ . Table 1 in the present paper summarizes this conversion and compares the resulting benchmark values with our numerical results obtained from the surface-charge solution and total-charge integration, Eq. (15). For representative slender cylinders ( $x = 10, 20, 50, 100$ , i. e.,  $\alpha = 0.1, 0.05, 0.02, 0.01$ ), the agreement remains at the sub-percent level, thereby providing an external validation of both the computed charge density on the lateral surface and the capacitance extraction procedure.

**Table 1:** Benchmark of the dimensionless capacitance for an open hollow conducting cylinder (lateral surface only). Reference values are taken from Table 1 of Ref. [13] (column  $C^{(H)}/a$ ) as a function  $x = L/a$ ; we use  $\alpha = a/L = 1/x$  to match our notation. To convert the Ref. [13] data to SI,  $C_{SI} = 4\pi\epsilon_0 a(C^{(H)}/a)$ ; equivalently, in our normalization  $\tilde{C}(\alpha) = C/(2\pi\epsilon_0 a) = 2(C^{(H)}/a)$ . The relative error reported in the last column is  $\Delta = \frac{|\tilde{C}_{[13]} - \tilde{C}_{\text{this work}}|}{\tilde{C}_{[13]}}$ . The agreement is at the sub-percent level over the tested aspect ratios.

$x = L/a$	$\alpha = a/L$	$C^{(H)}/a$ [13]	$\tilde{C}(\alpha) = (2/a)C^{(H)}$ [13]	This work	$\Delta(\%)$
10	0.1	2.479711	4.959422	4.960616	0.024
20	0.05	3.788663	7.577326	7.580178	0.038
50	0.02	7.092673	14.185346	14.195725	0.073
100	0.01	11.854900	23.709800	23.739575	0.126

The residual sub-percent discrepancies in Table 1 are expected and have two closely related origins. First, the benchmark values in Ref. [13] were obtained using a different high-precision numerical formulation (Love-type integral-equation methods and related schemes), whereas we solve an elliptic-kernel boundary integral equation using a Chebyshev-weighted parametrization combined with Nyström/collocation and panel quadrature. Since the two approaches rely on different discretizations, their truncation and quadrature errors are not identical. In our implementation the dominant numerical uncertainty is controlled by the finite-resolution parameters ( $N_c, n_g$ ) and by the accurate handling of the integrable rim singularity, which strongly influences convergence of the total-charge integral used to extract  $\tilde{C}(\alpha)$ , Eq. (15).

Second, the magnitude of the discrepancies is consistent with the finite- $N_c$  effects quantified independently in Sec. 4.1. As illustrated by the finite-size scaling analysis of the center density in Fig. 3 and the leading correction form Eq. (14), the  $N_c \rightarrow \infty$  extrapolation differs only weakly from the direct  $N_c = 220$  results. Because the capacitance is obtained from the same numerical charge density via a global integration, it inherits a discretization error of comparable order (set primarily by  $N_c$  at fixed  $n_g$ ). Therefore, the observed offsets in Table 1 are naturally attributed to residual  $\mathcal{O}(1/N_c)$  (and subleading  $\mathcal{O}(N_c^{-2})$ ) discretization errors in the numerical evaluation of the integral operator and in the rim-resolved charge integration, rather than to any systematic bias. Increasing  $N_c$  (or performing an explicit  $N_c \rightarrow \infty$  extrapolation for  $\tilde{C}(\alpha)$ ) would reduce the remaining differences further.

**Short cylinder ( $\alpha \gg 1$ )** In the extreme short-cylinder limit  $L \rightarrow 0$  (i. e.,  $\alpha = a/L \rightarrow \infty$ ), the lateral surface  $\rho = a$ ,  $|z| < L/2$  collapses geometrically to a ring-like object. Start from the axisymmetric Coulomb representation (1) of the surface potential on the lateral wall ( $\rho = a$ ) in terms of the longitudinal density  $\sigma(z)$ :

$$\Phi(a, z) = V_0 = k_e \int_{-L/2}^{L/2} a\sigma(z') dz' \int_0^{2\pi} \frac{d\varphi'}{\sqrt{(z - z')^2 + 2a^2 \sin^2(\varphi')}}. \quad (20)$$

The azimuthal integral is expressible through a complete elliptic integral and, for  $|z - z'| \ll a$  (which holds uniformly when  $L \ll a$ ) its standard near-singular expansion reduces the kernel to a logarithmic interaction along  $z$ :

$$\int_0^{2\pi} \frac{d\varphi'}{\sqrt{(z - z')^2 + 2a^2 \sin^2(\varphi')}} \simeq \frac{2}{a} \ln \left( \frac{8a}{|z - z'|} \right) + \mathcal{O} \left[ \frac{(z - z')^2}{a^3} \ln \left( \frac{8a}{|z - z'|} \right) \right]. \quad (21)$$

Hence, to leading order, the electrostatic potential satisfies

$$V_0 = 2k_e \int_{-L/2}^{L/2} \sigma(z') \ln \left( \frac{8a}{|z - z'|} \right) dz' + \text{subleading } \mathcal{O} \left[ (L/a)^2 \ln(a/L) \right]. \quad (22)$$

Introducing the dimensionless variable  $x = 2z/L \in [-1, 1]$  and motivated by the expected divergence of the surface-charge density at the cylinder ends, we adopt the leading-order *ansatz*

$$\sigma(z) \simeq \frac{A}{\sqrt{1 - x^2}}. \quad (23)$$

Using the classical identity for the logarithmic potential weighted by the Chebyshev measure [28],

$$\int_{-1}^1 \frac{\ln|x - x'|}{\sqrt{1 - x^2}} dx' = -\pi \ln 2, \quad |x| < 1. \quad (24)$$

and noting that  $|z - z'| = (L/2)|x - x'|$ , the integral equation reduces, at leading order and independently of  $x$ , to

$$V_0 = \frac{LA}{4\epsilon_0} \ln \left( \frac{32a}{L} \right). \quad (25)$$

Solving for the amplitude  $A$ , we obtain

$$A = \frac{4\epsilon_0 V_0}{L \ln(32a/L)}. \quad (26)$$

Substituting Eq. (26) into the ansatz (23), we find the dimensionless surface-charge density

$$\tilde{\sigma}(z) = \frac{a}{\epsilon_0 V_0} \sigma(z) \simeq \frac{4\alpha}{\ln(32\alpha)} \frac{1}{\sqrt{1 - x^2}}, \quad x = \frac{2z}{L}, \quad \alpha = \frac{a}{L} \gg 1. \quad (27)$$

Using the asymptotic expression (27), the total induced charge follows as

$$Q = \int_{-L/2}^{L/2} 2\pi a \sigma(z') dz' = 2\pi a \frac{L}{2} A \int_{-1}^1 \frac{dx}{\sqrt{1-x^2}} = \pi^2 a L A. \quad (28)$$

Consequently, the capacitance is given by

$$C = \frac{Q}{V_0} \simeq \frac{4\pi^2 \epsilon_0 a}{\ln(32\alpha)} \quad (L \ll a), \quad (29)$$

and, using the adimensional definition  $\tilde{C}(\alpha) = C/(2\pi\epsilon_0 a)$ , we finally obtain

$$\tilde{C}(\alpha) \simeq \frac{2\pi}{\ln(32\alpha)} \quad (\alpha \gg 1). \quad (30)$$

This asymptotic result was first obtained by Lebedev and Skal'skaya [11] using the method of dual integral equations.

This *logarithmic law* is consistent with the standard short-tube→ ring approximation reported in the capacitance literature for a hollow cylinder when the length is much smaller than the radius. In particular, several sources state a leading behavior of the form

$$C \propto \frac{a}{\ln(\text{const} \times L/a)}, \quad (31)$$

often written with a half-length notation  $\ell = L/2$ , leading to  $\ln(16a/\ell) = \ln(32a/L)$  [11]. High-precision computations for hollow cylinders also explicitly probe very small  $L/a$  and are consistent with this slow  $1/\ln(a/L)$  decay in the short-length regime [12–17].

A related but conceptually distinct approach to the evaluation of electrostatic energy and capacitance was recently proposed by Arun, et al. [18], who introduced an algebraic-topological method for computing stored electrostatic energy and three-dimensional Maxwellian capacitance in complex conductor configurations. Their framework emphasizes global topological invariants and network-based representations of the electrostatic field, offering an alternative to traditional boundary-integral or spectral formulations. In contrast, the present work focuses on a direct continuum description based on integral equations with physically transparent kernels, allowing for an explicit characterization of the surface-charge density and its singular behavior. Together, these complementary approaches highlight the diversity of available theoretical tools for capacitance evaluation and underscore the relevance of geometry-dependent effects in finite electrostatic systems.

However, for a zero-thickness conducting shell this limit is singular: the problem ceases to be a strictly two-dimensional surface-conductor boundary-value problem and effectively approaches a one-dimensional support, for which the notion of a smooth surface-charge density and a unique capacitance requires an additional transverse length scale. In practice, a physical “ring” is regularized by a finite wire radius or wall thickness (e.g., a *thin torus*), and the capacitance becomes finite but depends logarithmically on that transverse scale. Accordingly, while the ring-like interpretation is geometrically correct, the  $\alpha \rightarrow \infty$  limit of the present idealized

shell should be regarded as a formal asymptote rather than a universal, thickness-independent prediction; our numerical results are therefore intended for finite  $\alpha$ , where the shell model is well posed. Hence, we do not claim a universal  $\alpha \rightarrow \infty$  capacitance for the zero-thickness model; the asymptote is formal.

For the particular case of a toroidal conductor, with central radius  $a$  and a circular section of radius  $R$ , the dimensionless capacity is given by Refs. [25–27] as

$$\tilde{C} = \frac{8\pi}{a} \sqrt{a^2 - R^2} \left[ \frac{1}{2} \frac{Q_{-1/2}(a/R)}{P_{-1/2}(a/R)} + \sum_{n=1}^{\infty} \frac{Q_{n-1/2}(a/R)}{P_{n-1/2}(a/R)} \right], \quad (32)$$

where  $Q_s$  and  $P_s$  denote the Legendre functions of the first and second kind, respectively. We have adapted the original expression for the capacitance, given in Gaussian units, to the SI system. In our notation this corresponds to the transformation  $\tilde{C}(\alpha) = 2C_G/a$ , as discussed above.

The asymptotic expansion of (32), which is dominated by the lowest-order term, yields in the limit  $a \gg R = L/2$

$$\tilde{C}(\alpha) \simeq \frac{2\pi}{\ln(32\alpha)},$$

thereby confirming once again Eq.(30).

A caution is required in the opposite, short-cylinder regime: some tables approach a finite constant as  $\alpha \rightarrow \infty$ , which corresponds to a disk-like (end-cap-dominated) conductor with finite thickness. In our problem, the conductor is an open cylindrical shell (lateral surface only) with zero wall thickness; in this model, the short-cylinder limit is ring-like and singular, and a physical regularization requires an additional transverse length scale (wall thickness or wire radius). Therefore, only the slender-body entries ( $x \ll 1, \alpha \gg 1$ ) should be used for direct quantitative comparison with the present shell model.

#### 4.2.2 Capacitance Behavior Across Aspect Ratios

Figure 4 summarizes the numerical behavior of the dimensionless capacitance  $\tilde{C}(\alpha)$  over a broad range of aspect ratios  $\alpha = a/L$ . The results provide a smooth quantitative connection between the slender-cylinder limit  $\alpha \rightarrow 0$  ( $L \gg a$ ), where  $\tilde{C}(\alpha)$  grows rapidly and is well described by the classical Maxwell logarithmic asymptote in Eq. (18), and the short-cylinder limit  $\alpha \rightarrow \infty$  ( $L \ll a$ ), where the response becomes increasingly dominated by the rim regions and the dependence on geometry is only logarithmic. The inset, showing  $1/\tilde{C}(\alpha)$  versus  $\ln \alpha$ , makes this slow trend explicit and confirms the expected large- $\alpha$  behavior of the ideal zero-thickness shell, Eq. (30).

Beyond its pedagogical value, the present finite-length cylinder solution provides quantitative benchmarks for end-dominated electrostatics that are immediately useful in two applied settings. (i) **High-voltage hardware and feedthrough engineering:** breakdown and surface flashover are frequently initiated at geometric discontinuities (ends, triple-junction regions, and abrupt curvature changes) where the local field is enhanced; therefore, a controlled description of how the end singularity in  $\sigma(z)$  and the geometric capacitance  $C(\alpha)$  scale with aspect ratio offers a compact way to parameterize and validate design choices in high-voltage systems (including

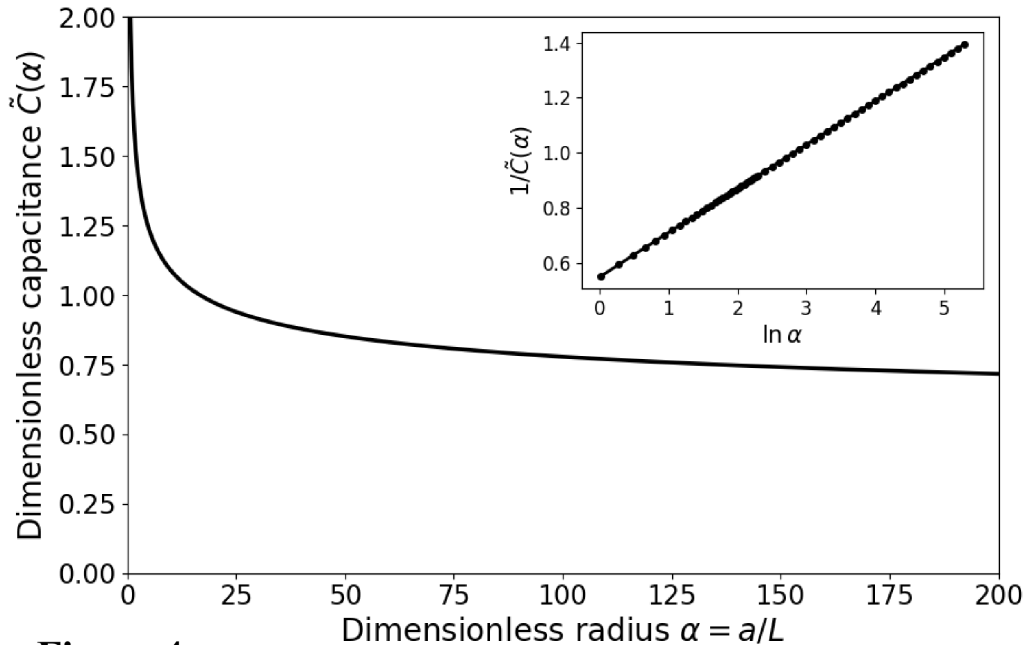


**Figure 4**

Figure 4: Dimensionless total capacitance of an open conducting cylinder (lateral surface only) held at a uniform potential  $V_0$ , shown as a function of the aspect parameter  $\alpha = a/L$ . The plotted quantity is  $C(\alpha)$  obtained from the numerically computed surface-charge distribution, Eq. (15). The vertical range is restricted to  $0 \leq C(\alpha) \leq 2.0$  to emphasize the rapid growth as  $\alpha \rightarrow 0$  (long-cylinder limit) while preserving detail at moderate  $\alpha$ . Inset:  $1/C(\alpha)$  versus  $\ln \alpha$ , emphasizing the slow logarithmic trend in the short-cylinder regime  $\alpha \gg 1$ , see Eq. (30).

electrode shaping and insulating feedthrough geometries) [29–33]. (ii) **Capacitance metrology and guarded electrode geometries:** guard-ring and re-entrant designs are employed precisely to suppress or correct fringing fields, and the residual fringing contribution is often the limiting systematic when cylindrical electrodes are used; thus,  $C(\alpha)$  and  $\sigma(z)$  supply geometry-resolved inputs for validating FEM/BEM corrections and for constructing/calibrating guarded standards and calculable-capacitor uncertainty budgets [34–37].

More broadly, the asymptotic form (18) quantifies the familiar “nearly linear” scaling of capacitance with length in slender conductors while making explicit the slow logarithmic correction that can matter at realistic aspect ratios. This correction is often invoked qualitatively in engineering approximations, but the present treatment offers a controlled bridge between the slender regime and the short, edge-dominated regime, providing a benchmark curve  $C(\alpha)$  that can be used to validate reduced models, boundary-element solvers, or simplified circuit representations of finite electrodes.

The capacitance provides a compact global characterization of the electrostatic response of the finite cylindrical conductor. Because it integrates the full surface-charge distribution, it is sensitive both to the bulk behavior and to the rim singularities discussed in the preceding asymptotic analysis. As such, the dependence of  $C(\alpha)$  on the aspect ratio offers a stringent diagnostic of the numerical solution and a natural way to connect the different physical regimes of the problem.

## 5 Spectral Formulation

Within the spectral approach, the electrostatic potential in the vacuum region outside the conducting cylindrical shell is represented by a Hankel (Fourier–Bessel) superposition of axisymmetric Laplace modes, namely

$$\Phi(\rho, z) = \int_0^\infty A(k) J_0(k\rho) e^{-k|z|} dk, \quad (33)$$

where  $A(k)$  is an a priori unknown spectral coefficient encoding the finite geometry of the conductor. This representation follows directly from separation of variables for the axisymmetric Laplace equation in cylindrical coordinates: for each transverse wavenumber  $k$ ,  $J_0(k\rho)$  provides the regular radial eigenfunction at  $\rho = 0$ , while the axial dependence  $e^{-k|z|}$  selects the decaying solution away from the plane  $z = 0$  and guarantees regularity at infinity. The absolute value  $|z|$  enforces the even symmetry in  $z$  appropriate to the present geometry, and the continuous integral over  $k$  reflects the unbounded radial domain. Closely related Hankel representations have been used in classical dual–integral–equation treatments of the hollow finite cylinder [4–8].

Imposing the boundary condition on the surface of the cylindrical shell,  $\Phi(a, z) = V_0$  for  $|z| < L/2$ , Eq. (33) reduces to the integral equation

$$\int_0^\infty A(k) J_0(ka) e^{-k|z|} dk = V_0, \quad |z| < L/2. \quad (34)$$

Equation (34) is a *Fredholm integral equation* of the first kind for the spectral coefficient  $A(k)$ . Because it is valid only on a finite interval of the axial coordinate, its inversion is nontrivial and, in the classical literature, leads to a coupled system of dual integral equations when supplemented with the regularity conditions outside the conductor [4–8].

Rather than determining  $A(k)$  directly, it is advantageous to relate it to the physically meaningful surface-charge density  $\sigma(z)$ . The latter is obtained from the normal derivative of the potential at the surface,

$$\sigma(z) = -\varepsilon_0 \frac{\partial \Phi}{\partial \rho} \bigg|_{\rho=a}. \quad (35)$$

Using Eq. (33) and the identity  $J'_0(k\rho) = -k J_1(k\rho)$ , one finds

$$\sigma(z) = \varepsilon_0 \int_0^\infty k A(k) J_1(ka) e^{-k|z|} dk, \quad (36)$$

where  $J_1(x)$  is the Bessel function of first order. Equation (36) shows that the spectral coefficient  $A(k)$  plays the role of a Laplace–Hankel transform of the surface-charge density. Formally inverting this relation, one may write

$$A(k) = \frac{1}{\varepsilon_0 J_1(ka)} \int_{-L/2}^{L/2} \sigma(z) e^{-k|z|} dk, \quad (37)$$

which expresses the spectral coefficient explicitly in terms of the unknown charge density  $\sigma(z)$ . This step is standard in spirit (it mirrors the classical dual-integral-equation constructions [7, 8]), but here we use it to eliminate  $A(k)$  entirely in favor of  $\sigma(z)$ .

Substituting Eq. (37) into the boundary condition (34) and interchanging the order of integration, we obtain a closed integral equation for  $\sigma(z)$ :

$$\int_{-L/2}^{L/2} \sigma(z') \left[ \int_0^\infty \frac{J_0(ka)}{J_1(ka)} e^{-k|z-z'|} dk \right] e^{-k|z|} dk = \varepsilon_0 V_0. \quad (38)$$

The problem is thus reduced, within the spectral framework, to a single real-space integral equation for  $\sigma(z)$ , with a kernel given by the inverse spectral integral in brackets. In the classical dual-integral-equation literature [7, 8], the analysis typically proceeds by manipulating Eq. (34)–(36) directly in Bessel space. Our aim here is different: we use the spectral representation only as a device to recover, in a systematic way, the same real-space operator that was obtained in Sec. 2 by direct ring-to-ring integration.

The kernel appearing in Eq. (38) can be evaluated explicitly using standard integral identities involving Bessel functions. In particular, one finds

$$\int_0^\infty \frac{J_0(ka)}{J_1(ka)} e^{-k|z-z'|} dk = \frac{1}{a} \frac{K\left(\frac{4a^2}{4a^2+(z-z')^2}\right)}{\sqrt{4a^2 + (z - z')^2}}, \quad (39)$$

where  $K(m)$  denotes the complete elliptic integral of the first kind, and the identity may be traced to standard tables of Bessel integrals [28]. Substitution of Eq. (39) into Eq. (38) yields precisely the real-space integral equation (5) derived earlier from ring-to-ring interactions. In other words, Eqs. (5) and (34) provide two mathematically equivalent formulations of the same electrostatic boundary-value problem: the former in terms of an elliptic kernel in physical space, the latter in terms of a spectral amplitude  $A(k)$  and dual integral equations.

The spectral formulation, based on Bessel-function expansions, emphasizes the modal structure of the solution and naturally leads to dual integral equations as in Refs. [4–8]. The real-space formulation, obtained here by explicitly eliminating the spectral coefficient and evaluating the Bessel integral, makes the nonlocal interaction along the cylindrical surface fully explicit through a kernel involving elliptic integrals. The equivalence between these approaches follows directly from the inversion of the Hankel–Laplace transform and demonstrates that the elliptic-integral kernel is nothing but the real-space representation of the underlying spectral operator. In both formulations, the finite length of the cylinder manifests itself through the singular behavior of the kernel, leading to an integrable divergence of the surface-charge density near the edges  $z = \pm L/2$ . This behavior is independent of the chosen representation and reflects the universal nature of edge effects in electrostatics. While both viewpoints appear separately in the literature, the present derivation provides an explicit elimination step that yields the elliptic kernel in closed form and is subsequently used in Sec. 3 to design a rim-aware discretization with controlled extrapolation.

## 6 Conclusion

In this work, we investigated the electrostatics of a thin conducting cylindrical shell of finite length maintained at a uniform potential. The problem was first formulated directly in real space, leading to an integral equation for the surface-charge density whose kernel is expressed in terms of complete elliptic integrals. This formulation provides a physically transparent description of the interaction between different axial elements of the conductor and proves to be particularly convenient for numerical implementation. The resulting charge distribution correctly captures the strong charge accumulation near the cylinder ends, as well as its dependence on the geometric aspect ratio  $L/a$ .

Subsequently, we revisited the same problem using a spectral representation of the electrostatic potential in terms of Bessel functions. By explicitly eliminating the spectral coefficient, we demonstrated the exact equivalence between the spectral formulation and the real-space integral equation with an elliptic kernel. This equivalence clarifies the relationship between two commonly employed but often separately presented approaches and shows that they are simply different representations of the same underlying electrostatic problem.

The numerical results obtained from the integral-equation approach allow for the accurate determination of the total induced charge and, consequently, of the capacitance of the finite conducting cylinder. Such configurations are of practical interest in a variety of applications, including the modeling of electrodes in vacuum devices, nanoscale conductive structures, cylindrical sensors, and components of capacitive energy-storage systems. Moreover, the methodology

developed here can be readily extended to more general boundary conditions, non-uniform potentials, or coupled multi-conductor geometries.

Overall, the present analysis provides a unified and consistent framework for the electrostatics of finite cylindrical conductors, combining physical transparency, mathematical rigor, and numerical efficiency. We expect that the equivalence established between the elliptic-kernel formulation and the spectral Bessel representation will be useful in both analytical studies and computational implementations of related electrostatic problems.

In addition to these possible extensions, the present results do more than solve a classical boundary-value problem: they supply benchmark-quality data for both the axial surface-charge profiles  $\sigma(z/L)$  and the dimensionless capacitance  $\tilde{C}(\alpha)$  over a wide range of aspect ratios. Because the rim singularity is built into the numerical ansatz and the convergence is quantified via finite-size scaling, these results provide a stringent test for high-accuracy boundary-element, finite-element, and method-of-moments solvers in electrostatics. In particular, any numerical scheme that aims to resolve edge fields on finite cylindrical conductors can be validated against the reference profiles reported here, both at the level of global observables (capacitance) and local behavior (near-edge charge build-up). In this sense, the finite conducting cylinder, equipped with the elliptic-kernel integral formulation and Chebyshev-weighted discretization, serves as a reusable benchmark geometry for future developments in computational electrostatics.

## Declaration of competing interest

The author declares that there are no known competing financial interests or personal relationships that could have appeared to influence the work reported in this paper.

## Acknowledgements

The author acknowledges the use of an AI-based language model (ChatGPT, OpenAI) to assist in improving the English language and clarity of some parts of this manuscript. All scientific content, results, and interpretations are the sole responsibility of the author.

## References

- [1] H. Cavendish, *The Electrical Researches*, Henry Cavendish (University Press, 1879).
- [2] J. C. Maxwell, *On the electrical capacity of a long narrow cylinder, and of a disk of sensible thickness*, *Proc. Lond. Math. Soc.* **9**, 94 (1877).
- [3] J. Lekner, *Electrostatics of conducting cylinders and spheres*, AIP Publishing, Melville, NY (2021).
- [4] L. Kapitsa, V. A. Fock, and L. A. Vainshtein, *Static boundary problems for a hollow cylinder of finite length*, *Zh. Tekh. Fiz.* **29**, 1177 (1959) [*Sov. Phys. Tech. Phys.* **4**, 1077 (1960)].

- [5] L. A. Vainshtein, *Static boundary problems for a hollow cylinder of finite length. II. Numerical results*, *Zh. Tekh. Fiz.* **32**, 1157 (1962) [*Sov. Phys. Tech. Phys.* **7**, 855 (1963)].
- [6] L. A. Vainshtein, *Static boundary problems for a hollow cylinder of finite length. III. Approximate formulas*, *Zh. Tekh. Fiz.* **32**, 1165 (1962) [*Sov. Phys. Tech. Phys.* **7**, 861 (1963)].
- [7] J. D. Jackson, *Charge density on thin straight wire, revisited*, *Am. J. Phys.* **68**, 789 (2000).
- [8] L. Verolino, *Capacitance of a hollow cylinder*, *Electr. Engin. (Berlin)* **78**, 201 (1995).
- [9] R. W. Scharstein, *Capacitance of a tube*, *J. Electrostatics* **65**, 21 (2007).
- [10] E. Romashets, M. Vandas, and C. Sen, *Capacitance of a conducting hollow cylindrical shell in a closed form*, *J. Electrostatics* **126**, 103866 (2013).
- [11] N. N. Lebedev and I. P. Skal'skaya, *Application of dual integral equations to the electrostatic problem of a hollow conducting cylinder of finite length*, *Sov. Phys.-Techn. Phys.* **18**, 28 (1973).
- [12] H. Gu, L. Huang, P. Yang, and T. Luo, *Capacitance of a Cube and a Hollow Cylinder*, *arXiv:2505.13148* (2025).
- [13] G. Paffuti, *Results for Capacitances and Forces in cylindrical systems*, *arXiv:1801.08202* (2018).
- [14] C. M. Butler, *Capacitance of a finite-length conducting cylindrical tube*, *J. Appl. Phys.* **51**, 5607 (1980).
- [15] J. Lekner, *Interior and exterior surface charge densities and quadrupole moment of an open conducting cylinder*, *J. Electrostatics* **136**, 104124 (2025).
- [16] W. R. Smythe, *Charged Right Circular Cylinder*, *J. Appl. Phys.* **27**, 917 (1956).
- [17] J. Lekner, *Interpolation formula for the capacitance of an open conducting cylinder*, *J. Electrostatics* **136**, 104132 (2025).
- [18] A. D. Arun, S. Chandra, S. Thirunavukkarasu, M. P. Rajiniganth, N. Malathi, and M. Sivaramakrishna, *A novel algebraic topological method-based approach for evaluating stored electrostatic energy and 3D Maxwellian capacitance*, *J. Electrostatics* **135**, 104065 (2025).
- [19] L. N. Trefethen, *Spectral Methods in MATLAB*, SIAM (2000).
- [20] J. P. Boyd, *Chebyshev and Fourier Spectral Methods*, Dover Publications, Dover Books on Mathematics, Mineola, NY (2001).
- [21] C. Canuto, M. Y. Hussaini, A. Quarteroni, and T. A. Zang, *Spectral Methods: Fundamentals in Single Domains*, Scientific Computation, Vol. 1, Berlin-Heidelberg, Springer (2006).

- [22] Rainer Kress, *Linear Integral Equations*, 3rd Edition, Applied Mathematical Sciences, Vol. 82, Springer, Cham (Switzerland), 2014.
- [23] K. Atkinson, *The Numerical Solution of Integral Equations of the Second Kind*, Cambridge University Press, Cambridge (1997).
- [24] J. Helsing and R. Ojala, *On the evaluation of layer potentials close to the boundary for Laplace's equation*, *J. Comput. Phys.* **227**, 2899 (2008).
- [25] W. M. Hicks, *On toroidal functions*, *Phil. Trans. Roy. Soc. London A* **31**, 609 (1881).
- [26] F. W. Dyson, *The Potential of an Anchor Ring*, *Phil. Trans. Roy. Soc. London* **184**, 43 (1893).
- [27] S. C. Loh, *The calculation of the electric potential and the capacity of a tore by means of toroidal functions*, *Can. J. Phys.* **37**, 698 (1959).
- [28] I. S. Gradshteyn and I. M. Ryzhik, *Table of integrals, series and products*, Academic Press, New York, 2007.
- [29] L. Chen, J. M. K. MacAlpine, X. Bian, L. Wang, and Z. Guan, *Comparison of methods for determining corona inception voltages of transmission line conductors*, *J. Electrostatics* **71**, 269 (2013).
- [30] J. R. Riba, C. Abomailek, P. Casals-Torrens, and F. Capelli, *Simplification and cost reduction of visual corona tests*, *IET Gen., Transm. & Distr.* **12**, 834 (2018).
- [31] A. L. Souza and I. J. S. Lopes, *Experimental investigation of corona onset in contaminated polymer surfaces*, *IEEE Trans. Diel. and Elec. Insul.* **22**, 1321 (2015).
- [32] J. D. Stein, *Compact high-voltage vacuum feedthrough*, *Rev. Sci. Instrum.* **47**, 1555 (1976).
- [33] W. C. Heerens and F. C. Vermeulen, *Capacitance of Kelvin guard-ring capacitors with modified edge geometry*, *J. Appl. Phys.* **46**, 2486 (1975).
- [34] A. M. Thompson and D. G. Lampard, *A New Theorem in Electrostatics and its Application to Calculable Standards of Capacitance*, *Nature* **177**, 888 (1956).
- [35] K. Jones and A. C. Corney, *The PEL Calculable Capacitor*, *Metrologia* **24**, 1 (1987).
- [36] W. K. Clothier, *A Calculable Standard of Capacitance*, *Metrologia* **1**, 36 (1965).
- [37] M. W. Keller, A. L. Eichenberger, J. M. Martinis, and N. M. Zimmerman, *Metrology triangle using a watt balance, a calculable capacitor and a single-electron tunnelling device*, *Metrologia* **45**, 330 (2008).